2D DC potential structures induced by RF sheaths coupled with transverse currents in front of ICRF antennas

Eric Faudot, S. Heuraux, L. Colas

2D potential structures induced by RF sheaths coupled with transverse currents in front of ICRH antenna

E. Faudot*, S. Heuraux*, L. Colas°

* LPMIA, UMR CNRS 7040, Universite Henri Poincare, Nancy 1
° Association Euratom-CEA pour la Fusion Controlee, CEA Cadarache

Abstract

Sheaths are space charge regions at the plasma-wall. They are induced by the differential inertia between ions and electrons, and without external perturbation, they create a floating potential between the neutral plasma and the walls. In Tokamaks, these sheaths are locally enhanced by the RF (radiofrequency) electric field generated by the ICRF (ion cyclotron resonance frequency) antennas used to heat magnetic fusion plasmas at very high temperature. RF sheaths are located at the connection points of magnetic field lines to the wall, or to the bumpers which protect the antenna or to any part of the antenna structure. The asymmetric behaviour of these oscillating sheaths rectifies RF potentials in the plasma in front of antenna, to finally create nonlinearly a DC potential which can be much higher than the floating potential. We study specifically how the space-time distribution of these RF and DC rectified potentials is modified when nearby flux tubes are allowed to exchange perpendicular polarization current. To simulate that, a 2D fluid code has been implemented to compute the 2D RF potential map in a plane perpendicular to magnetic lines, and within the flute approximation the whole 3D potential map is deduced. In simulation, we consider a homogeneous transverse conductivity and use a "test" potential map having, in absence of transverse currents, a Gaussian shape characterized by its width r0 and its amplitude ϕ_0. As a function of these 2 parameters (normalized respectively to a characteristic length for transverse transport and to the local temperature), we can estimate the peaking and the smoothing of the potential structure in the presence of polarization current. So, we are able to determine, for typical plasmas, the amplitude of DC potential peaks , particularly on antenna's corners , where hot spots appear during a shot. In typical Tore Supra conditions near antenna corners potential structures less than centimetric are involved in the 2D effects. The next step will consist in studying space transition between several areas characterized by different perpendicular conductivities, which can be modelled via effective connection lengths in our 2D fluid code. This more precise approach will be useful to obtain the potential structures in front of each part of the complex antenna's geometry and to minimize potential peaks generating many spurious perturbations in the plasma edge for long duration discharge as in ITER reactor.

1 Introduction

The study of 2D potential structures in front of ICRH antenna has been firstly motivated by the apparition, on antenna structure, of hot spots [1] [2] in the upper left hand corner or in the lower right hand corner with respect to magnetic field direction (see fig. 1). The main component of RF electric field radiated by the antenna straps is along y (poloïdal direction). The integration of the projection of these electric fields along the magnetic lines between the 2 bumpers gives a non null RF electrostatic potential [3]. Magnetic lines can be seen as flux tubes ended by RF sheaths which rectify the RF potential and are able to create high DC potential structures in front the Faraday screen of antenna. These structures can then accelerate parallel ion fluxes and convective fluxes on to the antenna's surface and dangerously heat the materials to finally create hot spots. The rectification of RF potential due to sheaths [4] and parallel dynamic of rf sheaths [5] have been studied in previous works. Other approaches have taken into account transverse currents in fluid models, in case of Langmuir probes [10] [7] [8] with an approximation of scale lengths for currents [9] and in case of edge plasma in Tokamak [11]. But closer papers concerns RF sheaths driven by ICRH modelized with a fluid model [12] [13] [14]. In our case, RF potentials will be rectified by sheaths and due to non uniform electric fields, flux tubes could be polarized differently in the vicinity of the antenna. These potential gradients will create some perpendicular currents and consequently modify the flux tube RF and DC polarization [15]. The purpose here is to evaluate quantitatively and self-consistently the rectified potential dynamics due to transverse polarization currents and, then to apply it to a real case. So, firstly we are going to deal with a "flux tube model with transverse polarization currents", next we will be interested in analytic calculations compared to numeric computation of the rectified potential. Then we will be able to define a potential peak criterion depending on plasma parameters. And finally, we will analyse interactions between magnetic lines with different lengths.

2 Modelling and analytical RF rectified potential with transverse currents

2.1 Basic description of RF sheaths

To model potential behaviours in front of antenna, we need one flux tube able to exchange current with its neighbour. This flux tube represents the plasma along an open magnetic field line (OMFL) situated between antenna's bumpers in our particular case. The sheaths appear at the ends of an OMFL, in a small layer near the material surface of the bumpers represented by electrodes. Now, if we consider that electrodes at each end of the magnetic line play a symetrical role, we obtain the electric model by putting the ground "in the middle" of the circuit (see fig 2). The choice of the mass position is crucial. For instance, if only one electrode is directly connected to the ground, the amplitude of the rectified potential in the plasma will be double (see section 3.3). Here, we have made the choice of a symetric circuit,

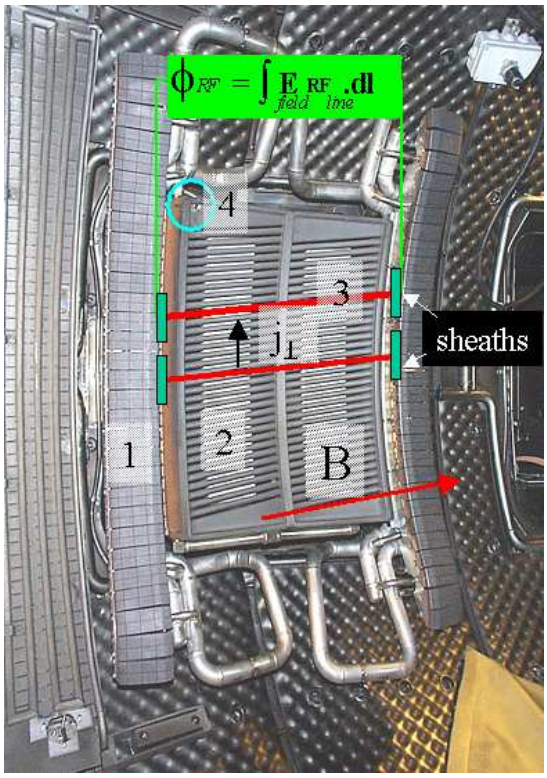

Figure 1: The hot spot appears (4) on the upper left hand corner of the Faraday screen. Magnetic lines(3) and sheaths are represented in front of the antenna [1]. (1) and (2) are respectively the bumpers protecting the antenna and the straps radiating the waves

because it seems to be the most realistic configuration, nevertheless a rigourous demonstration has to be done to define the importance of the masss in case of RF sheath driven by RF electric fields. From this point, we make the assumptions that, of course, the model is electrostatic and $\omega < \omega_{pi}$, so that we can neglect the parallel dynamic of the sheath. Moreover, plasma density is supposed to be constant, and electrons follow Boltzmann law. One can now apply current conservation with a double probe model to which we have added transverse current to obtain the expression 2.

$$\nabla.(j_\parallel + j_\perp) = 0 \tag{1}$$

$j_\parallel$ is the parallel density current and $j_\perp$ is the transverse density current
The Bolzmann electronic density distribution $n_0.exp(\frac{eV}{kT_e})$ associated to $j_{isat} = e.n_0.C_s$ leads to the I-V characteristic for a probe and after integration over one flux tube : $j_{isat} - j_{esat}exp(-\phi + \phi_{RF}/2) + j_{isat} - j_{esat}exp(-\phi - \phi_{RF}/2) + L_\parallel \nabla j_\perp = 0$, j_{isat} and j_{esat} are respectively ionic and electronic saturation current, ϕ the potential of the plasma compared to the mass, ϕ_{RF} the RF potential resulting from the integration of the parallel electric field E_{RF} along an OMFL. For all calculus, ϕ and ϕ_{RF} are normalized to $\frac{kT_e}{e}$, and depend of the time t and the spatial coordinate r in a cylindrical geometry. The $\parallel$ direction is along B_0 and the $\perp$ direction is perpendicular to B_0.

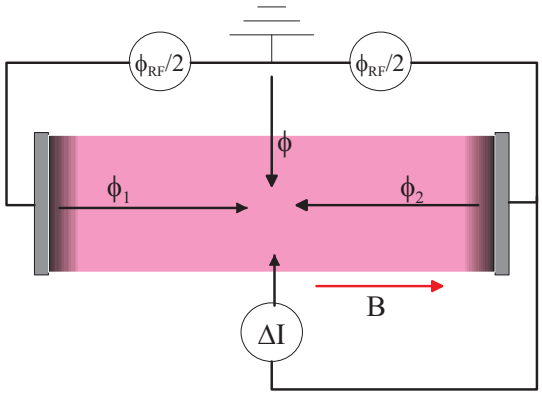

Figure 2: Scheme of 1 flux tube model with transverse current.

$$\frac{j_{esat}}{2j_{isat}}(exp(\phi_{RF}/2)+exp(-\phi_{RF}/2))=(1-\frac{L_{\parallel}\nabla j_{\perp}}{2j_{isat}})exp(\phi) \tag{2}$$

2.2 fluid model

The purpose here is to extend the flux tube model to a fluid model. Thus, we introduce the transport term for transverse current ΔI. We must now evaluate ΔI which can be collisionnal or non collisionnal (polarization current).

$$\Delta I=-L_{\parallel}\nabla_{\perp}.j_{\perp}=L_{\parallel}(\sigma_{col}+\sigma_{pol})\nabla^2\phi$$

$L_{\parallel}$ is the OMFL length, σ_{col} and σ_{pol} are respectively the perpendicular collisional and polarization conductivity. From momentum equation, we deduce each component :

$\sigma_{col}=\frac{n_0.e^2}{m_i\nu_i(1+\frac{\Omega_{ci}}{\nu_i^2})}+\frac{n_0.e^2}{m_e\nu_e(1+\frac{\Omega_{ce}}{\nu_e^2})}$ $\qquad$ $\sigma_{pol}=i\frac{n_0e^2}{m_i}\frac{\omega}{\Omega_{ci}^2-\omega^2}+i\frac{n_0e^2}{m_e}\frac{\omega}{\Omega_{ce}^2-\omega^2}$

n_0 the plasma density, e the electron charge, m_i the ion mass, ν_i the ion-ion collision frequency, m_e the electron mass, ν_e the electron-ion collision frequency, Ω_{ci} the ion cycloton pulsation and Ω_{ce} the electron cyclotron pulsation and ω is the pulsation of ϕ_{RF}.

$\omega_{ci}<<\omega_{ce}$, so σ_{pol} is simplified for a homogeneous plasma, the convection term, and the electronic part are neglected : $\sigma_{pol}\approx\frac{n_0e^2}{m_i\Omega_{ci}^2}\frac{\partial}{\partial t}$. In our working conditions $\sigma_{col}<<\sigma_{pol}$ so that it is suppressed from the global expression for the transverse current: $\frac{\Delta I}{2j_{isat}}=\frac{L_{\parallel}\rho_s}{2\Omega_{ci}}\frac{\partial\nabla^2\phi}{\partial t}$, where ρ_s is the ion Larmor radius. For the following calculus we will work on a spatial Gaussian potential structure which oscillates with a pusation ω in a cylindrical geometry.

$\phi_{float}=\log(\frac{j_{esat}}{j_{isat}})$ $\qquad$ $\phi_{RF}(r,t)=\phi_0.cos(\omega t)exp(-\frac{r^2}{r_0^2})$ $\qquad$ $A=\frac{L_{\parallel}\rho_s}{2\Omega_{ci}}$

We deduce the expression of the rectified potential structure from equation 2 :

$$\boxed{\phi(r,t)=\phi_{float}+ln(ch(\frac{\phi_{RF}(r,t)}{2}))-ln(1-A\frac{\partial\nabla^2\phi(0,t)}{\partial t})} \tag{3}$$

where ϕ_{float} is the floating potential of the plasma.

3 physical regimes of the dynamic system

The discussion on the different regimes will depend on the 3 characteristic parameters : $\omega\tau_\perp$ the "characteristic relaxation time" , $\frac{L_{nc}^2}{r_0^2}$ equivalent to $\omega\tau_\perp$ and ϕ_0 the amplitude of $\phi_{RF}(r,t)$, with $\tau_\perp = -4\frac{A}{r_0^2}$ and $L_{nc} = \omega A$.

3.1 linear regime

If $\omega\tau_\perp\phi_0 << 1$, then the expression can be linearized

$$\phi_{lin} = \phi_{float} + ln(ch(\phi_{RF}/2)) + \delta\phi_{lin} \tag{4}$$

with $\delta\phi_{lin} = A\frac{\partial\nabla^2\phi(0,t)}{\partial t} = 4\frac{L_{nc}^2}{r_0^2}(\frac{r^2}{r_0^2} - 1)\phi_0 sign(\cos(\omega t))\sin(\omega t)\exp(-\frac{r^2}{r_0^2})$
In that case, the time average potential of maximum of the gaussian structure is $< \phi >_t = \int_0^{2\pi}\phi_{lin}d\omega t = \frac{\phi_0}{\pi} - ln(2)$ because the contribution of the time average linearized term is null.
For $L_{nc}^2 \ll r_0^2$, $\phi \approx \phi_{float} + ln(ch(\phi_{RF}/2)) + \delta\phi_{lin}$. Temporaly, $\phi(0,t) \approx \phi_{float} + ln(ch(\phi_{RF}(0,t)/2))$. Spatially, gaussian potential structure will be modified. A short analyse permits to say, according to the signs of $\delta\phi$, that in the ascending phase ($\phi_{RF}/2$ for $\omega t = [\frac{\pi}{2};\pi]$) the top part of the structure ($r = [0;r_0]$ convex part) is reduced and contracted, and increased and dilated in the low part ($r = [r_0;\infty]$ concave part). In contrary, in descending phase ($\omega t = [0;\frac{\pi}{2}]$), top part is increased and dilated and low part is reduced and contracted. The maximum typical diffusion length during a period is of the order of L_{nc}. The linear analyse in Fourier space for the first harmonic gives an evaluation of the new gaussian width. The gaussian structure is replaced by a parabole whose the base width is ΔL. We obtain one part in phase with ϕ_{RF} , this is $\Delta L_0 \approx r_0(1 + 32L_{nc}^4/r_0^4)$ and another contribution in quadrature $\Delta L_{\frac{\pi}{2}} \approx r_0(\sqrt{2}/2)(1 + 48L_{nc}^4/r_0^4)$.

For $L_{nc}^2 \gg r_0^2$, temporaly, $\phi(0,t) \approx \phi_{float} + ln(ch(\phi_{RF}(0,t)/2)) + \delta\phi(0,t)$. Spatially, using the same method than in the former case,
$\Delta L_0 \approx L_{nc}(\omega)\sqrt{\pi/ln(2L_{nc}/r_0)}$ and $\Delta L_{\frac{\pi}{2}} \approx r_0\sqrt{(2\ln(2L_{nc}/r_0)}$

For $\omega\tau_\perp\phi_0 = 1$, we can extract the criteria that defines the linear/non linear limit.

3.2 non linear regime

If $\omega\tau_\perp\phi_0 >> 1$, the expression becomes strongly non linear. The spatial behaviour for the potential structure remains the same than in linearized model, but due to logarithm, the reduction-contraction effect is minimized in ascending phase for the top part and in descending phase for the low part, while increasing-dilatation effect is amplified in descending phase for the top part and in ascending phase for the low part.

Temporaly, we suppose that the summit of the potential structure remains Gaussian even in non linear case : $\Delta\phi(0,t) = \frac{-4}{r_0^2}\phi(0,t)$.

$$\phi(0,t) = \phi_{float} + ln(ch(\phi_{RF}/2)) - \delta\phi_{nolin}(0,t) \quad (5)$$

with $\delta\phi_{nolin}(0,t) = \ln(1 - \tau_\perp \frac{\partial\phi(0,t)}{\partial t})$

While $\phi < \phi_{float} + ln(ch(\phi_{RF}/2))$, the $\delta\phi_{nolin}$ is positive and weak compared to its linear expression, ϕ follows $\phi_{float} + ln(ch(\phi_{RF}/2))$. Next, when ϕ passes over the sollicitation the $\delta\phi_{nolin}$ becomes negative and so strong that the summit of the structure relaxes slowly as a capacitive relaxation. In that case we can consider the extreme case for which the current saturates, that is to say $\frac{\partial}{\partial t}\phi(0,t)) = -1/\tau_\perp$. Here the slope of the summit evolution becomes constant and equal to $-1/\tau_\perp$ (see fig. 3). We are now able to evaluate the amplitude of the oscillating part of the signal $\tilde{\phi} \rightarrow \frac{\pi}{\omega\tau_\perp} << \phi_0$ in non linear regime. The first consequence is that asymptoticaly, $< \phi >_t \rightarrow \phi_0/2$, because the time inertia of the potential structure is so strong that the structure does not move a lot during one period.
Spatially, it is too difficult to evaluate the non linear diffusive behaviour of the structure. We can only say that for $L_{nc}^2 \ll r_0^2$ the structure is quasi not modified and for $L_{nc}^2 \gg r_0^2$ the base of the structure is widened with a fraction of L_{nc} and the top part remains non diffused and conserves the amplitude of the order of the sollicitation $\phi_{RF}/2$.

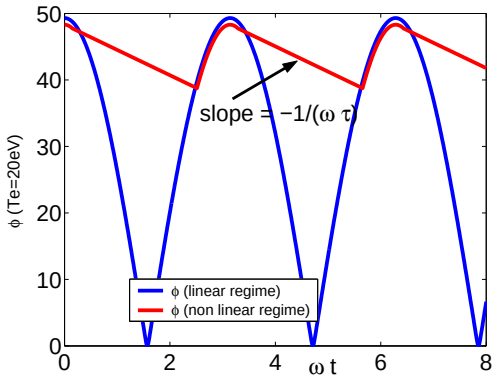

Figure 3: linear and non linear rectified potential amplitude with transverse current

3.3 analytical expression for the non linear rectified potential

From the expression 2 with the assumptions of expression 5, we obtain the expression below which can be integrated :

$$\int_0^{wt} \alpha\Big(exp(\phi_{RF}(0,t)/2) + exp(-\phi_{RF}(0,t)/2)\Big)dwt = \int_0^{wt} \Big(1 + \tau_\perp \frac{\partial\phi}{\partial wt}\Big)exp(\phi)dwt$$

Then, we introduce Bessel functions to achieve the integration as following :

$\int_0^{wt} exp(\frac{\phi_0}{2}.cos(\omega t) + \frac{wt}{\tau_\perp})d\omega t = \int_0^{wt} \Big(I_0(\frac{\phi_0}{2}) + 2\sum_{k=1}^{\infty} I_k(\frac{\phi_0}{2})cos(k.wt)\Big)exp(\frac{wt}{\tau_\perp})dwt$

And we finally obtain the analytic expression for $\phi(0,t)$ in a non linear case with the assumption $\Delta\phi(0,t) = \frac{-4}{r_0^2}\phi(0,t)$ (gaussian shape is conserved in the top part of the structure).

$$\phi(0,t) = \log\Big[exp(-\frac{wt}{\tau_\perp}))\Big(1 - \alpha(\beta + 2\sum_{k=1}^{\infty}\gamma)\Big)\Big] + \tilde{\phi}(0,t) \tag{6}$$

$$\text{with } \beta = I_0(\tfrac{\phi_0}{2}) + I_0(\tfrac{-\phi_0}{2}),\ \gamma = \tfrac{I_k(\frac{\phi_0}{2}) + I_k(\frac{-\phi_0}{2})}{1+\tau_\perp^2 k^2}$$
$$\text{and } \tilde{\phi}(0,t) = \alpha\Big(\beta + 2\tau_\perp \textstyle\sum_{k=1}^{\infty}\gamma(\tau_\perp^{-1}cos(k.wt) + k.sin(k.wt))\Big)$$

If we had chosen to connect one electrode of our model to the ground, we would have obtained the same expression for ϕ, but with $\beta = 1 + I_0(\phi_0)$ instead of $I_0(\frac{\phi_0}{2}) + I_0(\frac{-\phi_0}{2})$ and with $\gamma = \frac{I_k(\phi_0)}{1+\tau_\perp^2 k^2}$ instead of $\frac{I_k(\frac{\phi_0}{2}) + I_k(\frac{-\phi_0}{2})}{1+\tau_\perp^2 k^2}$. If the oscillating part is not taken into account in expression 6, then $< \phi >_t \rightarrow \phi_0/2$, while in case of the mass connected to one electrode, $< \phi >_t \rightarrow \phi_0$. Moreover, it could be noted that without transverse currents $< \phi >_t \rightarrow \phi_0/\pi$. In the first case, the plasma is driven by an extern homogeneous RF electric field with symetrical electrodes, and in the second case, the plasma is driven by the polarization of one electrode. That is why the way we treat our circuit leads to results separated by a factor 2. So, it is important to know in reality the position of the ground, in other words , which rôle plays the RF potential distribution on the rectified potential along a magnetic line. This problem could be developped in another work.

4 Numeric simulations of RF rectified potential in a poloïdal plan in front of ICRH antenna and results comparison

While analytical study seems to approach very closely temporal amplitude of the potential structure, a numerical resolution of the fluid model is needed to evaluate precisely spatial and temporal potential structure in a plan perpendicular to the antenna Faraday screen (poloïdal plan). Parallel potential gradients are null except in the sheath. The simulation area is a grid composed of 256x256 cells. One cell is shorter than L_{nc}, and $dt = 10^{-11}s$ smaller than Ω_{ci}^{-1} [15].

4.1 Rectified potential signal and time average structure

The purpose of the first set of simulations was to confirm the validity of our analytical model and in the same time to validate the good behaviour of our code. As in analytical part, we use here a RF sinusoïdal and gaussian potential structure $\phi_{RF} = \phi_0.cos(\omega t)exp(\frac{-(x^2+y^2)}{r_0^2})$ placed in the centre of our grid.

For $\omega\tau_\perp\phi_0 < 1$, the linearized model described in expression 4 can be applied, and figure 4 on the left shows that the temporal inertia of the potential structure is

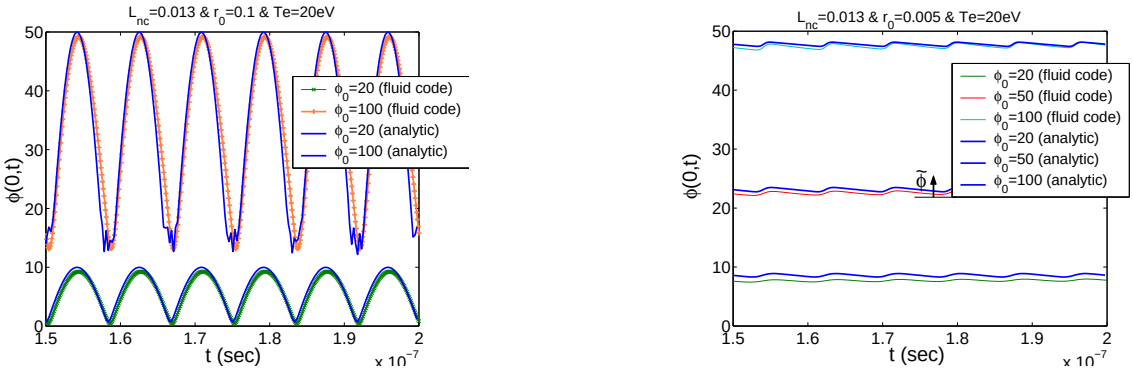

Figure 4: These 2 figures represent the amplitude of the gaussian structure with respect to time for 3 and 2 values of RF potential $\phi_{RF} = \phi_0 exp(-r^2/r_0^2) sin(\omega t)$ and for 2 values of $\omega\tau_{perp} = 4\frac{L_{nc}^2}{r_0^2}$ ($\omega\tau_\perp = 0.017$, linear behaviour, and $\omega\tau_\perp = 6.7$, non linear behaviour)

weak in descending phase. Here the non linear analytical expression 6 is also valid (see figure 4). Here tranverse current effects are negligible and $< \phi >_t \rightarrow \phi_0/\pi$.

For $\omega\tau_\perp\phi_0 > 1$, the figure 4 on the right reveals the good agreement between the code and non linear analytic expression 6 for $\phi(0,t)$. One more time, we establish here that in one hand, $max(\phi(0,t)) \approx \phi_0/2$, and in the other hand, $\tilde{\phi} \rightarrow \pi/\tau_\perp$. In fact, the main effect of RF sheath is to rectify the potential signal. As for the transverse current, it makes the time average value grow until $\phi_0/2$ when $\omega\tau_\perp\phi_0 \rightarrow \infty$.

Spatially, For $L_{nc}^2 > r_0^2$, so for a diffusion length greater than potential structure width, on the figure 5 the widening of the base of the time averaged structure is visible and of the order of L_{nc}, whereas the upper part is increased as it has been said previously (see part 3.2). For $L_{nc}^2 < r_0^2$, the widening is less visible on figure 5 but the structure is modified in the same way.

From these results, now we are going to use the simulation possibilities to obtain a peak criterion to be compared to the one coming from analytical and non linear expression 6.

4.2 peak criterion

The parametric study consist of testing how the time averaged potential amplitude is rectified with respect to the 2 parameters ϕ_0, the initial RF potential amplitude and $\omega\tau_\perp$ the relaxing normalized time of the potential structure. So by spreading ϕ_0 in a range from 1 to 100 and $\omega\tau_\perp$ from .01 to 10, we obtain iso curves which give the peaking ratio equal to the time averaged amplitude of the potential structure without currents over the maximum amplitude of RF potential.

The first conclusion about this criterion is the good agrement between code and analytical results except for $< \phi(0,t) >_t /\phi_0 = 0.45$. This is simply due to the quality of the interpolation obtained with a finite number of simulations. Secondly, as unexpected it could be, structures are not smoothed in the sense of a

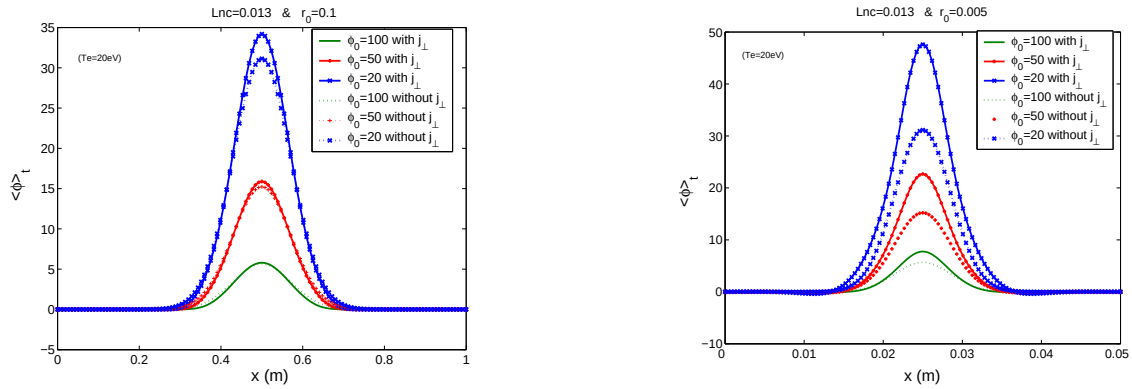

Figure 5: These 2 figures represent the spatial distribution of the time averaged rectified gaussian structure for 3 values of RF potential $\phi_{RF} = \phi_0 exp(-r^2/r_0^2) sin(\omega t)$ and for 2 values of $\omega\tau_{perp} = 4\frac{L_{nc}^2}{r_0^2}$ ($\omega\tau_\perp = 0.017$, linear behaviour, and $\omega\tau_\perp = 6.7$, non linear behaviour.)

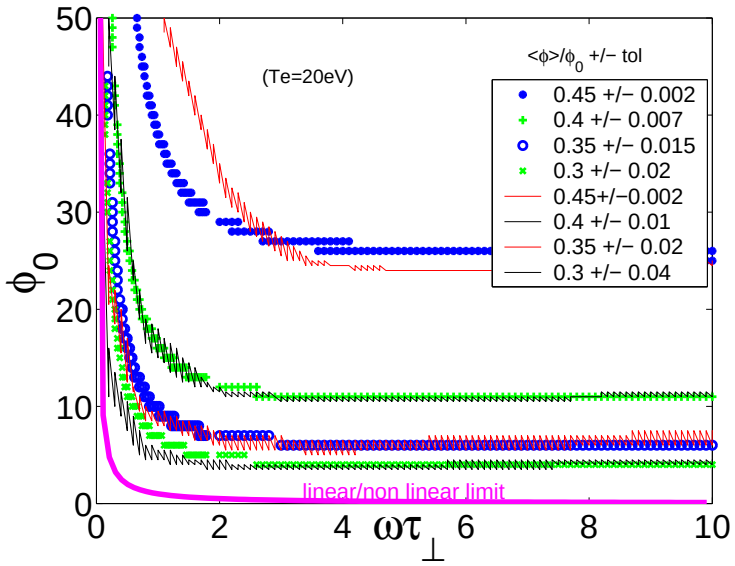

Figure 6: This figure gives the typical domain for Tore Supra's antenna compared to iso curves corresponding to the ratio of the time average peaked structure over the amplitude of ϕ_{RF}. This, with respect to the parameter $\omega\tau = -4\frac{L_{nc}^2}{r_0^2}$ corresponding to the temporal inertia of the potential structure or to its width compared to L_{nc}.

pure diffusion. In contrary, they are peaked in the upper part, and dilated in the lower part. All these observations are made by using the time average value of the amplitude and the spatial distribution during a period. And thirdly, typical Tore Supra potential structures are centimetric wide ($0.2 < \omega\tau_\perp < 4$) and their amplitude are in a range from 100 to 1000 volts ($5 < \phi_0 < 50$). These parameters come from the potential map computed by the code ICANT [16] (see fig. 7), and so are mainly concerned by our non linear theory, which will be very usefull to firstly evaluate the

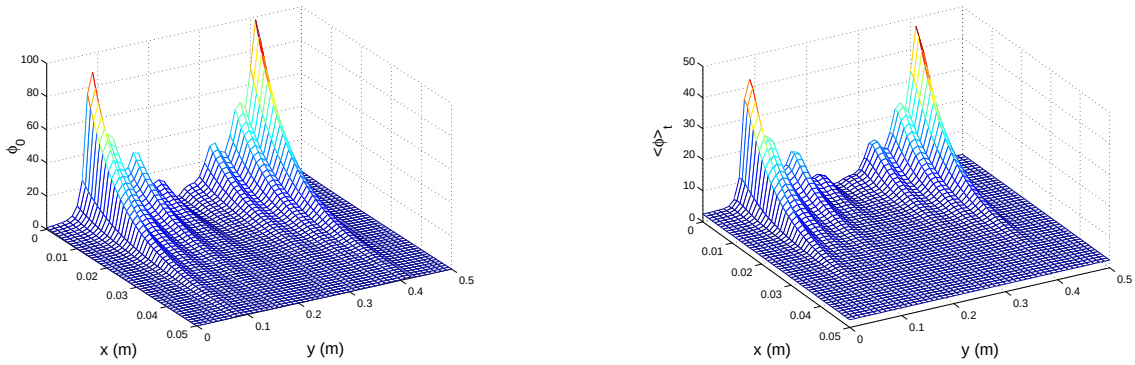

Figure 7: On the left is the RF potential map computed by the ICANT code in poloidal plane in front of ICRF antenna. On the right, this is the DC rectified potential map but with transverse current effects.

amplitude of potential structure able to create high localized convective fluxes. We can see on figure 7 that 2 potential peaks are situated at the top and bottom part of the antenna, which could explain why hot spots often appear in these areas , and particularly in the corners depending on magnetic field direction.

5 First approach of current interactions between different magnetic line lengths for a non linear case

The whole potential map in front of ICRH antenna was previously obtained [15] using the integration of parallel electric fields given by the code ICANT. This was done by considering that all magnetic lines between the bumpers had the same lengths. In fact, in the corner of antenna, magnetic lines between both the bumpers can exchange currents with ones between one bumper and the wall or a limiter of the Tokamak. We have observed before than a long flux tube has more temporal inertia than a short one because $\tau_\perp = \frac{L_\parallel \rho_s}{2\Omega_{ci}}$. This will be the case here. Starting from the same model than in section 2, we can add a flux tube composed of 2 sub-flux-tubes to finally obtain the scheme of the figure 8.

Here transverse currents are supposed to be conserved : $L_{1\parallel}\nabla j_\perp = L_{2\parallel}\nabla j_{1\perp} + L_{3\parallel}\nabla j_{2\perp}$. The potential gradients are null along z but they are not null along x and y, because of the RF gaussian potential structure we use here again. These gradients appear on figure 8 thanks to $\phi_{RF}/2$ equivalent to $\phi_{RF}(x_0, y_0, t)/2$ and $\phi'_{RF}/2$ equivalent to $\phi_{RF}(x_0, y_1, t)/2$. In that case, the gaussian structure is applied to 2 domains corresponding to the "long line 1" or to the "composed line 2 and 3". These 2 domains are separated by $x = 0.5x_{max}$. So left half part of the structure will concern the "long line domain" and the left half part will concern either "the short line 2" or "the complementary line 3". That is why we measure the potential map in 2 positions along z (see figure 8). These 2 potential maps appear on figure 5. Then

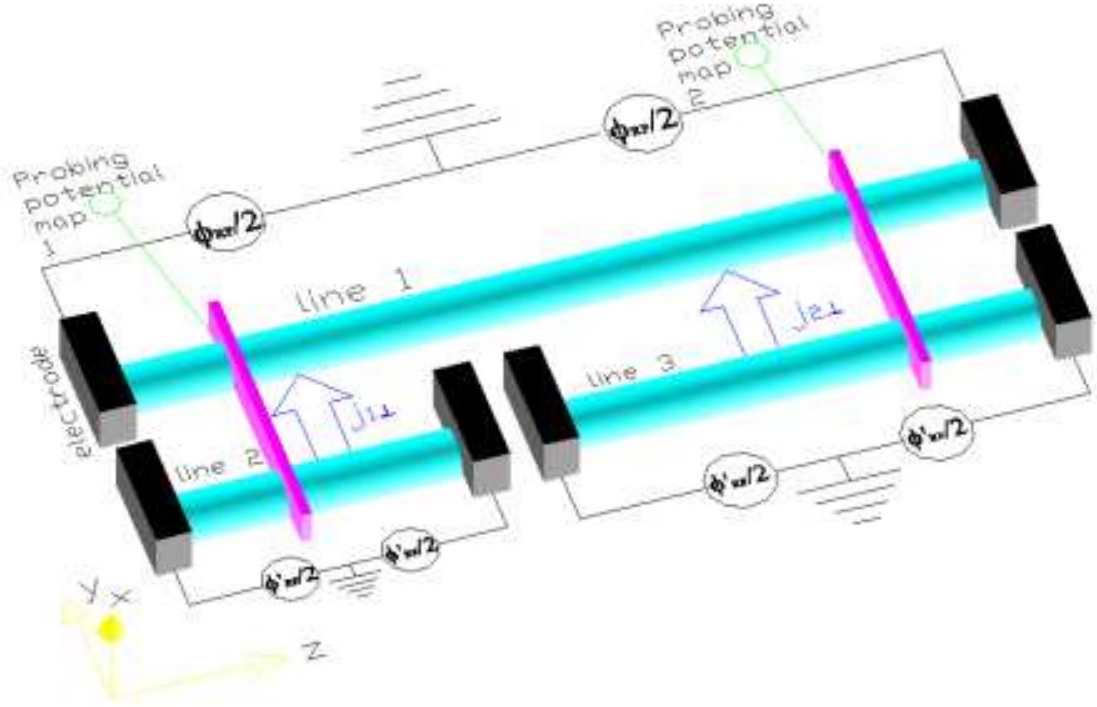

Figure 8: The figure above shows a 3 flux tubes model built like the one flux tube model of figure 2. The flux tube 1 (line 1) is polarized with $\phi_{RF}/2$ and both flux tubes 2 and 3 (line 2 et 3) are polarized with $\phi'_{RF}/2$. $j_{1\perp}$ and $j_{2\perp}$ are respectively the transverse currents exchanged between lines 1 and 2, and between lines 1 and 3.

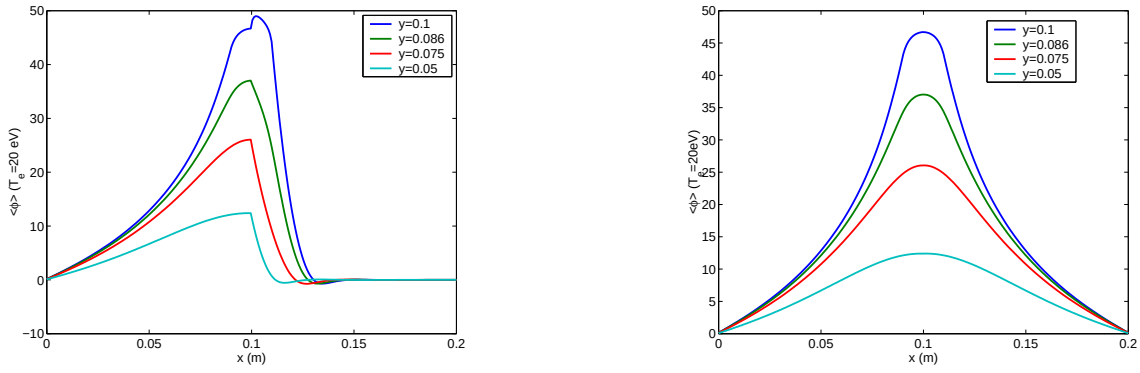

Figure 9: Both figures represent the time average potential structure with respect to coordinate x. The left one is the potential map 1 probed by the 1st wall on scheme 8 and the right one is the potential map 2 probed by the second wall on scheme 8.

we observe that for $L_{1\parallel} = 1$, $L_{2\parallel} = 0.01$ and $L_{1\parallel} = 0.99$, the boundary between $L_{1\parallel}$ and $L_{3\parallel}$ is indiscernible. On contrary, we see the boundary between $L_{1\parallel}$ and $L_{2\parallel}$. For the moment, we are just able to explain qualitatively this observation. In fact, the different line lengths influence the temporal inertia and the diffusion of the potential

structure. So, spatially, the graf on the left on figure 5 shows that on the side of the "short line" , the widening of the structure is weak ($L_{nc} \ll r_0$) as expected whereas it is very strong on the left hand side because $L_{nc} \gg r_0$. Temporaly, problem is more subtle because if we look at the summit of the structure, which represents the time average amplitude, we can notice that each maximum at the boundary are not so far. For instance, the average amplitude for the "short line" would have been ϕ_0/π in case of a homogeneous "short line" map. Here, the time average amplitude is quasi equal the "long line" one ($\phi_0/2$). Then, this seems to demonstrate that the dynamic of the "short line" follows the "long line" one. Now the next step of our work will consist to evaluate the equivalent line length of a "short line" close from a "long line" with respect to their 2 lengths (see prospects).

6 conclusion

The elaboration of a simple flux tube model able to exchange transverse polarization currents leads us to obtain an analytical expression for the rectified potential of the open magnetic field lines (OMFL) in front of ICRF antenna. We deduced from the linearized expression of ϕ, that the time average potential with and without current is the same : $\phi_{DC} = \phi_0/\pi$. Spatially we evaluate the widening of the structure which is a fraction of L_{nc}. From the non linear expression of ϕ, with the assumption that the top of the structure is still a Gaussian, we have evaluated the relaxation time $\tau_\perp$, similar to the one used for a capacitive charge. When $\omega\tau_\perp\phi_0 \gg 1$, then $\phi_{DC} \to \phi_0/2$, but the spatial widening of gaussian potential structure is not easy to obtain. These results were in good agreement with those of our 2D fluid code confirming that the assumption of $\nabla^2\phi(0,t) = -4/r_0^2\phi(0,t)$ is good. The code permits to obtain a potential peak criterion demonstrating that the typical Tore Supra potential structures have a non linear behaviour so that their DC amplitude will be increased. So the time average of a high RF potential will give a high DC potential able to accelerate ions and convective fluxes. All these results have been obtained for same OMFL length. That is why, we explore the case of interaction between different OMFL lengths. And first simulations seem to show that transverse currents make a short line temporal dynamic follow the dynamic of a long one. But, obviously, such a work has to be developped to test more complex configurations like in the corners of antenna, and at the boundary of the bumpers or limiters.

References

[1] L. Colas and al: Nuclear Fusion 43 (2003) 1-15

[2] M. Becoulet and al. : Plasma Physics 9, 2619 (2002)

[3] J-M Noterdaeme and G. Van Oost : Plasma Phys. Control. Fusion 35 (1993) 1481-1511

[4] V.A. Godyak and A.A. Kuzovnikov : Fiz. Plazmy 1,496-503 (May-June 1975)

[5] J-J. Gonzalez and A. Shabalin : Plasma Sources Sci. Technol. 12 (2003) 317-323

[6] V. Rozhansky and al.: Contrib. Plasma Phys. 36 (1996) 2/3, 391-395

[7] K. Gunther, A. Carlson Contrib. Plasma Phys 34 (1994) 2/3, 484-489

[8] M. Ashraf and M.G. Rusbridge, Plasma Physics and Controlled Fusion, Vol. 29 (1987), No 8, 969-992

[9] A. Carlson : Phys. Plasmas, Vol.8, No. 11, November 2001

[10] V. Rozhansky and al.: Contrib. Plasma Phys. 36 (1996) 2/3, 391-395

[11] V.A. Rozhansky and al. : Nucl. Fusion 41 No. 4

[12] D.A. D'Ippolito and al : Phys. Fluids B 5 (10), October 1993

[13] D.A. D'Ippolito and J.R. Myra : Physics of plasmas, Volume 7, number 8, August 2000

[14] D.A. D'Ippolito and al : Nucl. Fusion 42 (2002) 1357-1365

[15] E. Faudot and al. : Czech. J. Phys. 53 (2003), Vol. 53, October 2003, No. 10

[16] S. Pecoul and al : Comp. Phys. Comm. 146 (2002), 166-187